Arab J Geosci
DOI 10.1007/s12517-013-0937-y

ORIGINAL PAPER

Mapping subvertical discontinuities in rock cuts using a 400-MHz ground penetrating radar antenna

Adnan Aqeel · Neil Anderson · Norbert Maerz

Received: 4 January 2013 / Accepted: 15 March 2013

Abstract Hidden subvertical discontinuities oriented parallel to subparallel to the exposed faces of outcropping sandstone were effectively mapped at three different study sites in central Missouri using a ground-penetrating radar system (GPR) equipped with a 400-MHz monostatic antenna and a survey wheel. At each site, a suite of 2-D ground-penetrating radar profiles were acquired along multiple closely spaced traverses on relatively smooth exposed rock surfaces. Time-zero correction was applied to the raw GPR data which were then processed using band-pass filtering, range and display gain, color transformation, and deconvolution techniques. Pseudo 3D images of each identified discontinuity at each site were constructed based on the interpretation of the nonmigrated ground-penetrating radar profiles. These pseudo 3D images were hand-migrated and transformed into true 3D images which depict variable depths at "perpendicular horizontal distance" to each discontinuity relative to the exposed rock face. The results demonstrate that GPR can be used to detect and map hidden discontinuities. This information can then be used for rock slope stability analysis and rock engineering purposes.

Keywords Ground-penetrating radar · Subvertical discontinuities · Sandstone rock cut · "Perpendicular horizontal depth" · Migration

Introduction

A rock mass is usually characterized by the presence of discontinuities that divide the rock mass into different sized blocks of intact rocks. Discontinuities occur either naturally or by blasting.

Discontinuity is a general term which implies a natural or man-made break in the continuity of a rock fabric without referring to its genetic origin (Scheidegger 1978; Otoo et al. 2011a; Aqeel 2012). A discontinuity has generally no tensile strength with low shear strength and high fluid conductivity when compared to the intact rock itself (Chernyshev and Dearman 1991; Priest 1993).

Recent studies show that even where the strength of intact rock is high, the probability of failure may also be high because of the presence of discontinuities in rock mass (Slob et al. 2004, 2005). Accordingly, the mechanical and hydrological behavior of a rock mass is largely controlled and governed by the geometry of its discontinuities (Bieniawski 1989; Kiliche 1999; Otoo et al. 2011b).

A discontinuity within a rock mass, exposed in an outcrop or rock cut,, manifests itself in one of two ways as shown in Fig. 1:

- either as a fracture trace (a visible line) on the rock-cut surface due to the intersection of the plane of the discontinuity and the plane of the rock-cut face
- or as an exposed plane or face on the rock-cut surface on which can be considered to be like "facet" on a precious cut stone (Duan et al. 2011; Otoo et al. 2011a). Both of the two ways of exposure for discontinuities can be seen on the same rock cut (Fig. 1).

Discontinuities can be mapped on rock masses using a traditional manual method like as a scanline, or, more recently, using light detection and ranging methods (Post 2001; Slob and Hack 2004; Donovan et al. 2005; Haneberg 2008; Sturzeinegger and Stead 2009; Otoo et al. 2011a). However, only visible discontinuities in rock mass can be measured and mapped in this manner. Vertical or subvertical discontinuities that strike parallel or semi-parallel to the rock mass face and are not exposed cannot be mapped using these methods. This can lead to underestimation of the potential for slope failures and disasters such

A. Aqeel · N. Anderson · N. Maerz
Department of Geological Sciences and Engineering, Missouri University of Science and Technology, 1006 Kings highway, Rolla, MO 65409-0660, USA

A. Aqeel (✉)
Department of Earth and Environmental Sciences, Sana'a University, Sana'a, Yemen
e-mail: ben_aqeel_2005@yahoo.com

Published online: 30 April 2013

Fig. 1 A rock cut showing both discontinuity traces as lines and discontinuity facets as polygons

as the rock slide that occurred in Al-Dhafir village in Sana'a Governorate, Yemen, in December 28, 2008 (Fig. 2). Therefore, detecting and mapping visually hidden discontinuities is a necessary step for proper rock slope stability evaluation.

In some cases, horizontal drilling can be used to identify hidden discontinuities, but that is a time-consuming and expensive process that often requires one or more lane closures. Recently, ground-penetrating radar (GPR) has been effectively used to detect and map hidden discontinuities (Maerz and Kim 2000; Soel et al. 2001; Porsani et al. 2006). The main objective of this study is to detect and map hidden subvertical discontinuities in three dimensions and demonstrate that a more accurate image of hidden discontinuities can help in terms of rock slope stability evaluation and rock failure mode definition.

Study area location

The study area is a quartz sandstone outcrop located adjacent to Interstate 44, northwest of the city of Rolla in Phelps County, Missouri, USA. The outcrop, consisting of Roubidoux Sandstone Formation, lies between 37° 56′21″ and 37° 56′26″N and 091° 48′23″ and 091° 48′39″W.

The outcrop was divided into three sites for investigation purposes. Each site (station) can be considered to be an individual rock cut (Fig. 3). The height of the rock cut at each of these three stations ranges between 2.40 and 4.00 m, while the widths average about 3.00 m. All the three stations which are smooth rock-cut surfaces across ground-penetrating radar data were easily and effectively acquired.

GPR data acquisition

The terms "ground-penetrating radar" (GPR) and "georadar" refer to a range of electromagnetic tools designed primarily to map buried objects or interfaces that are buried beneath the ground surface or located within a visually opaque structure (Daniels 2004) or discontinuities located behind rock slope or cut face. GPR has become enormously popular, specifically within the engineering community since the mid-1980s; however, GPR has been used for geological investigations since the 1960s, especially in connection with the development of radar echo sounding of polar ice sheets (Reynolds John 1997).

GPR is an active noninvasive geophysical method for commonly nondestructive subsurface imaging and based on the propagation of electromagnetic waves in the subsurface and earth materials (Daniels 2004; Conyers 2004; Otto and Sass 2006; Sass 2007).

Fig. 2 A catastrophic rock slide happened along hidden subvertical discontinuity and destroyed tens of houses and killed 65 persons in Al-Dhafir village in Sana'a, Yemen, in 2008 (retrieved from Aqeel 2012)

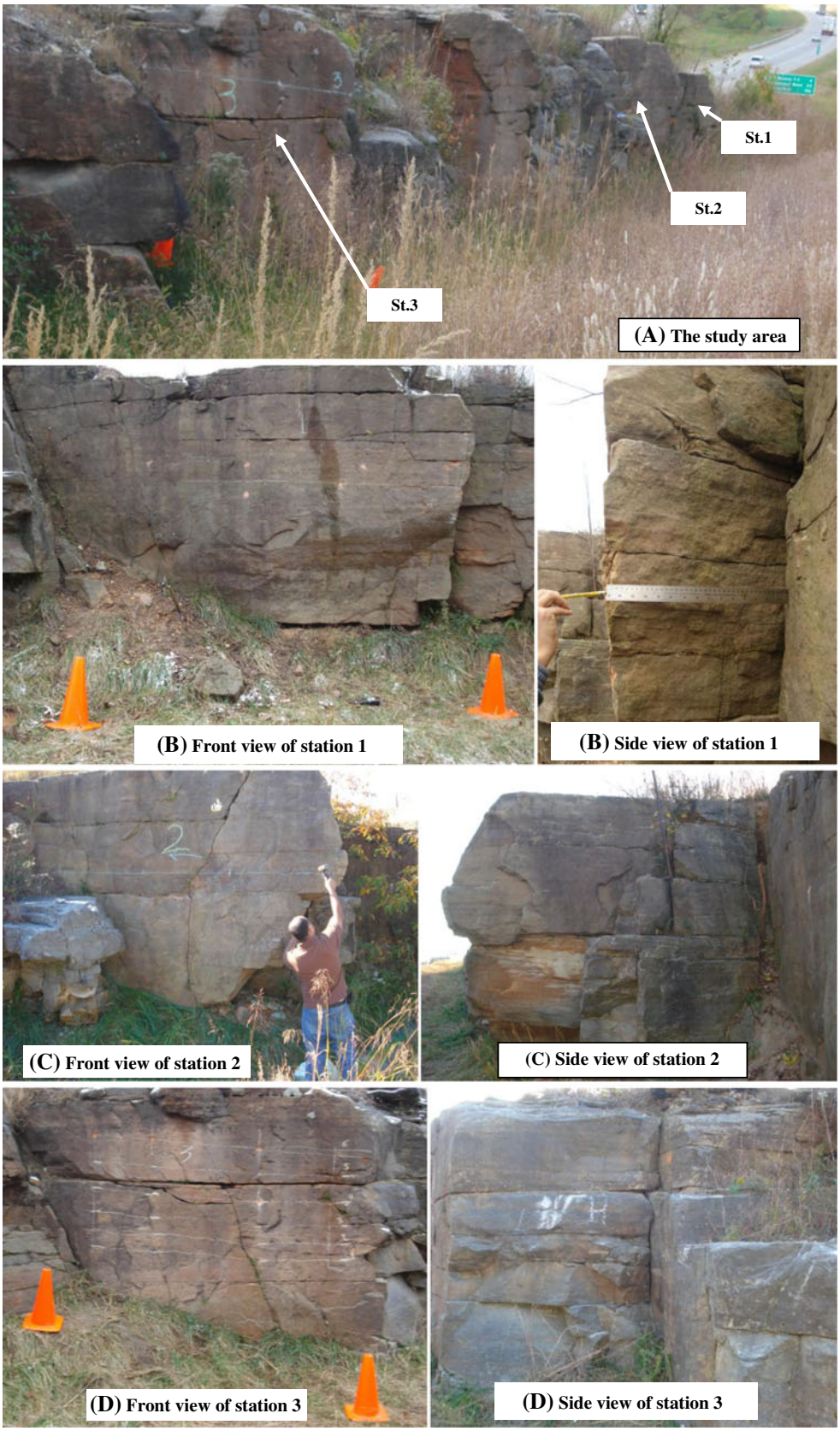

Fig. 3 The study area was divided into three stations or rock cuts as shown in *a*: station 1 (*b*), station 2 (*c*) on which the author is standing as a scale and conducting field work, and station 3 (*d*)

GPR is typically used to investigate and detect subsurface targets or objects such as discontinuities whose electrical properties differ from those of surrounding environment. Parameters of either reflections from subsurface interfaces

Fig. 4 A wheel was attached to the used 400-MHz GPR monostatic antenna to acquire the data in distance mode while towing the antenna on rock-cut faces

or transmitted electromagnetic waves are employed to study the dielectric properties of the subsurface features. Some physical properties of subsurface target(s) such as its nature and components (discontinuity, in-filled-discontinuity, buried metal, rock, soil, etc.), electrical conductivity, magnetic permeability, and more specific relative dielectric permittivity in addition to the type and the frequency of the used antenna have to be taken into consideration for a better understanding on GPR data (Aqeel 2012).

GPR product, which is a radiogram image, is not only an image of the subsurface but is the recorded response of the subsurface materials to the propagation of electromagnetic energy in the microwave range and across a relatively narrow range of radio waves with frequencies of, typically, 10 MHz and over 1.5 GHz (Takahashi 2004; Booth et al. 2009; Cassidy 2009a).

An Impulse SIR-3000 GPR system which is manufactured by Geophysical Survey Systems, Inc. (GSSI) was used during this investigation. The resolution of the acquired GPR data and the penetration depth of GPR waves are mainly controlled mostly by the frequency of the antenna. Higher-frequency antenna produces higher-resolution data but provide shallower depths of investigation. Lower-frequency antenna is capable of imaging the subsurface to greater depths but produce lower-resolution images (Beres and Haeni 1991; Kovin and Anderson 2005, 2006; Otto and Sass 2006).

Table 1 The geometry of the three stations (rock-cut faces) in the study area

Rock cut (station) no.	Dip direction	Dip angle
1	028°	73°
2	022°	85°
3	22°	87°

Generally, a 1,500-MHz antenna is capable to image the subsurface within less than a 0.5-m depth, whereas a 900-MHz antenna can image the subsurface up to a 1-m depth, assuming a relative dielectric permittivity of 5. However, in this research, the objective was to detect and map discontinuities in rock cuts at depths (distances) shallower than 3 m. Discontinuities at depths (distances) greater than 4 m are of less concern because gravity and the unit weight of the intact rocks located deeply behind the rock-cut face will function as stabilization factors. Maerz and Kim (2000) employed three different antennae at 1,500, 900, and 400 MHz to identify the discontinuities in highway sandstone rock cuts in Missouri. They found that only 400-MHz antenna waves penetrated deeply enough into the rock cut to clearly identify the discontinuities to depths about 3 m. Moreover, Kovin (2010) found that utilizing a 400-MHz antenna can

Fig. 5 Towing the 400-MHz GPR antenna on the rock-cut surface of station 2 after fastening the wheel. The work needed at least three people to carry on the field work. The author is standing in the middle observing the process of acquiring GPR data and recording notes

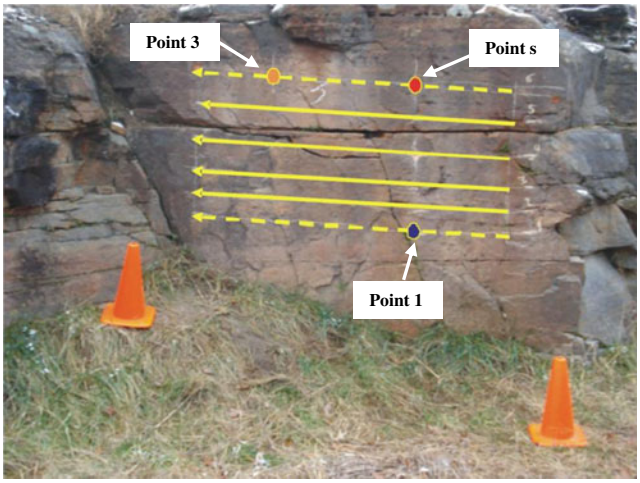

Fig. 6 Parallel horizontal GPR survey lines (*dashed lines* are the two lines passed through the three marked points on the rock-cut face) which are parallel to the strike direction of the plane of the rock-cut face of station 3

effectively image fractures within about 4 m of depths in a salty rock.

Accordingly, a 400-MHz monostatic GPR antenna was used in this research as it provided both the prerequisite depths of investigation and the required GPR data resolution. A survey wheel was attached to the GPR antenna so that the data could be acquired at uniform intervals along each traverse (Figs. 4 and 5). The following steps were followed at and for each station:

1. The geometry of rock-cut faces (dip direction and dip angle) was measured using a Brunton compass (Table 1).
2. On each rock-cut face, three slightly coplanar marks (index points) were created using a hammer. These marks served as fixed reference points. On photographs, index point 1 is distinguished by small blue circle, while index points 2 and 3 are distinguished by small red and orange circles, respectively
3. These three index points represent fixed locations on the rock slope faces from which the apparent and the true perpendicular depths (distances) to the detected hidden subvertical joints were measured using GPR images (radiograms).
4. From these three marked points, "true perpendicular horizontal distances" (referred to as vertical depth in the geophysical literatures) to the detected hidden subvertical discontinuities were estimated.
5. Several horizontal GPR survey profiles were acquired at each station and used to create the 3D radiogram images shown in Fig. 3(d). Two of these the GPR profiles passed through the three marked points on each rock-cut face. However, to distinguish these two GPR profiles from the other profiles, their traverse locations were drawn as dashed lines as illustrated in Fig. 6. In this research, the index point 2 and the index point 3 are located on the same GPR profiles, while the index point 1 is located on a separate GPR profile. The spacing between GPR profiles varied between 12 and 22 cm depending on the geometry, the appearance, and the smoothness of each rock-cut face.

Estimation of GPR pulse velocity

An intact rock sample was collected from the study area and used to measure the GPR velocity of the sandstone. The rock sample was trimmed into two rectangular blocks using a large-diameter diamond-saw blade. The two sandstone blocks became wet after the sawing process, so they were dried by putting them in an oven under a temperature of 100 °C for about 20 h. Then, the blocks were cooled to room temperature for couple of hours prior to the start of the lab test.

Laboratory velocity tests utilizing a 1,500-MHz GPR monostatic antenna were conducted on the two sandstone blocks. To simulate natural conditions, the two rock blocks were positioned on top each other with a separation of 1.80 cm between them to act as a discontinuity plane (Fig. 7). The purpose was to measure a highly accurate GPR pulse velocity and to estimate the relative dielectric permittivity of the dry rock sample. When GPR velocity is

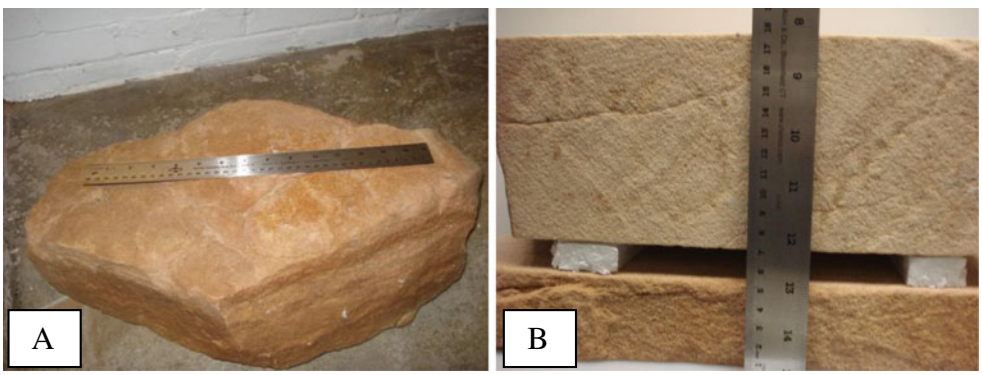

Fig. 7 **a** The collected raw sandstone sample from the study area. **b** The created two sandstone blocks with a separation acting as a discontinuity surface. The thickness of the top block is 10.60 cm, while the separation between the two blocks is 1.80 cm

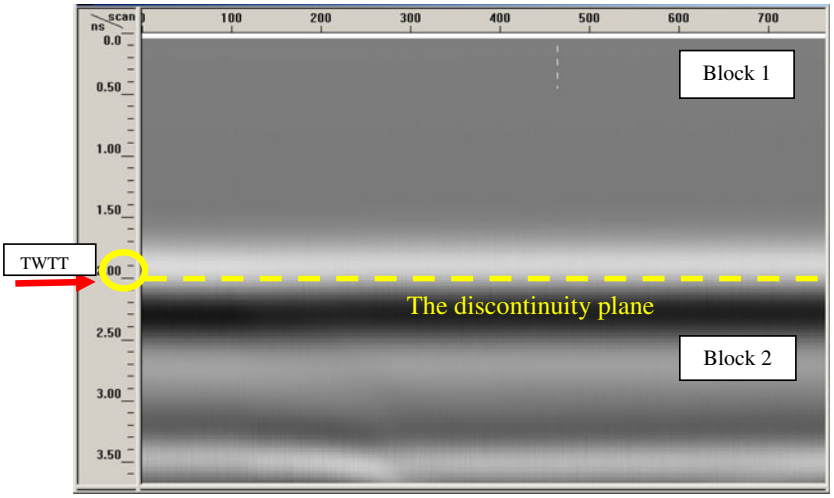

Fig. 8 The radiogram image shows that the two-way travel time from the surface of the top block (block 1) to the discontinuity plane location (*dashed line*) was 2 ns

estimated, true perpendicular horizontal depths (distances) to detected subvertical discontinuities in the rock cuts can be determined.

A 1,500-MHz GSSI-GPR monostatic antenna was moved across the surface of the top rock block in order to map the artificial discontinuity plane. This test was repeated twice to assure repeatability of data and reliability of results. The zero correction and display gain process were applied to the resulting radiogram images to enhance the resolution and the clarity of the images. As shown in Fig. 7, the thickness of the top block was 10.60 cm, which means that the true calculated perpendicular depth (d) to the artificial discontinuity plane has to be 10.60 cm.

The resulting radiogram image showed that the two-way travel time (t) of the GPR pulses was 2 ns as illustrated in Fig. 8. When the vertical axis (Y-axis) of the radiogram was set in a depth mode in the monitor of the GPR system, the radiogram image showed that the perpendicular (vertical) depth to the discontinuity was 10.60 cm, which reflects the accuracy and the precision of the input parameters in the used GPR system and, thus, the work and the results as listed in Table 2 and shown in Fig. 9. From the resulted two radiogram images (Figs. 8 and 9),

- the two-way travel time = 2 ns = t
- the perpendicular (vertical) depth = 10.60 cm=0.106 m = d

Table 2 The parameters which were entered into the GPR system of the 1,500-GHz monostatic antenna to estimate the velocity of the GPR pulses in sandstone sample collected from Roubidoux Outcrop, Rolla, MO

Parameter	Value
Sample	512
Bits	16
Range	13 ns
Dielectric	8
Rate	100
Sample/unit	2 scan/cm

by using the equation

$$V = 2d/t \tag{1}$$

The velocity of GPR pulses that pass through that sandstone of the study area is 0.106 m/ns. Now, the relative dielectric permittivity of the sandstone sample can be measured using the following equation:

$$V = c\Big/(\varepsilon)^{1/2} \tag{2}$$

where c is the speed of light in a vacuum in meters per nanosecond. Thus, the relative dielectric permittivity of the sandstone (ε) is estimated to be 8. Hence, the perpendicular depth can be estimated to any detected discontinuity in GPR data record either from resulting radiograms (using a dielectric permittivity of 8) or manually using the following equation:

$$d = (0.15 * t)\Big/(\varepsilon)^{1/2} \tag{3}$$

A dielectric value (ε=8) will be suitable for interpreting the GPR Rubidoux Sandstone data acquired in the study area.

GPR data processing

The main purpose of GPR data processing is to make data interpretation easier and more reliable, which is basically achieved by improving the raw data quality (Cassidy 2009a). A Radar Data Analyzer software package (RADANTM) which is produced by GSSI was used for GPR data processing. After the position correction (zero or time-offset correction) step for acquired GPR data, it is common, as a first step in GPR data processing techniques, to filter the data. The main goal of GPR data filter technique is to focus the radiogram image and to improve the visual

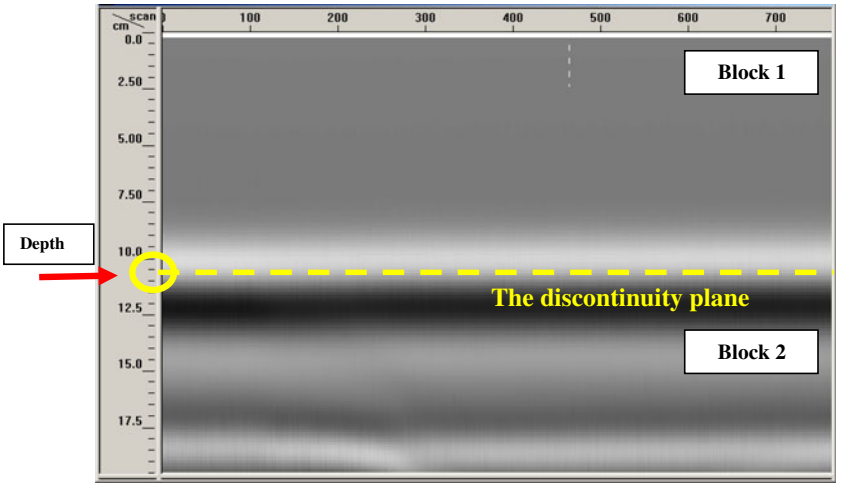

Fig. 9 The measured true perpendicular (vertical) depth to the artificial discontinuity surface is 10.60 cm as shown in the radiogram image

quality of the data by removing instrumentation noise from data (Reynolds 1997; Annan 2009; Cassidy 2009b).

Infinite impulse response (IIR) filtering was used. A 800-MHz vertical low pass filter was used to remove high frequency, while a 100-MHz vertical high pass filter was used to remove potential flat-laying ringing system noise. However, the IIR filtering method generally has a limited noise reduction; therefore, the color transformation of a value of 17 was used to hide what little noise may remain in the acquired GPR data. For many GPR applications, filtering method is sufficient to locate subsurface features (Reynolds 1997; Annan 2009). However, the main concern in this research is to map sufficiently hidden discontinuities, which are small in terms of width, opening aperture. Consequently, it is needed to maximize the resolution and improve the visual quality of the data as possible. Hence, range and display gain and deconvolution techniques were applied. The purpose of deconvolution is normally to maximize bandwidth and reduce GPR pulse dispersion to ultimately maximize resolution. Operator length of 31, prediction lag of 5, pre-whitening of 10 %, and with an overall gain of 1 were used as parameters for the deconvolution method. Figures 10 and 11 are displays of raw and processed GPR data acquired along the two GPR profiles that pass through the three marked points at each station.

The geometrical relationship between the detected hidden discontinuities and the rock-cut face is very important in order to identify potential rock failure modes especially toppling and/or plane rock failure types. Subsequently, migration of the GPR data was a necessary step in order to reconstruct the true geometry of the detected hidden discontinuities, and thus, to estimate the true depths (true horizontal perpendicular distances) form the three marked/index points on each rock-cut face to the detected hidden discontinuities at that rock cut.

Migration is commonly the final step in the processing of the GPR user. It is used to create more spatially realistic images of the subsurface (Cassidy 2009b). Migration is simply a mathematical process which can be done using specialized software or manually. GPR data migration by using software is usually successful in relatively homogenous environments such as pavements and glacial environments. However, it tends to be less successful for complex and heterogeneous sites (Cassidy 2009b). Therefore, manual migration was used in this research to avoid uncertainty that could result from variability in the inherent properties of the hidden discontinuities.

Once the GPR pulse velocity and the relative dielectric permittivity for a rock cut were measured, the two-way travel times can be translated to depths, and then migration could be applied (Reynolds 1997; Aqeel 2012). The 2D GPR images along each profile or traverse can be imagined as a horizontal plane penetrating the rock-cut face. The mapped discontinuities can be thought of as intersecting this 2D plane, resulting in an intersection line which can be considered as "the strike line" of this detected discontinuity. This strike line appears as a linear feature (reflector, interface, or even) on the GPR radiogram as shown in Figs. 10 and 11.

For a dipping discontinuity, migration process results in the apparent dip angle of a slopping discontinuity being corrected to a steeper angle (Cassidy 2009a, b). Manual migration, which was used in this research, for GPR data is explained in many geophysical references (Kleyn 1983; Jenyon and Fitch 1985; Lines and Newrick 2004; Conyers 2004; Aqeel 2012).

Manual migration was done for all detected hidden subvertical discontinuities in the study area using GPR radiogram images and based on the following equation:

$$\sin \beta = \tan \alpha \tag{4}$$

where

β the true declination angle of the strike line of the detected hidden subvertical discontinuity

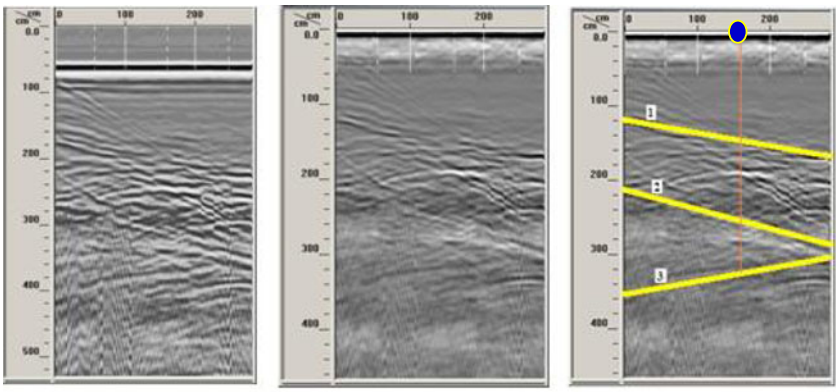

(A) Raw and processed GPR profile 2 at Station 1

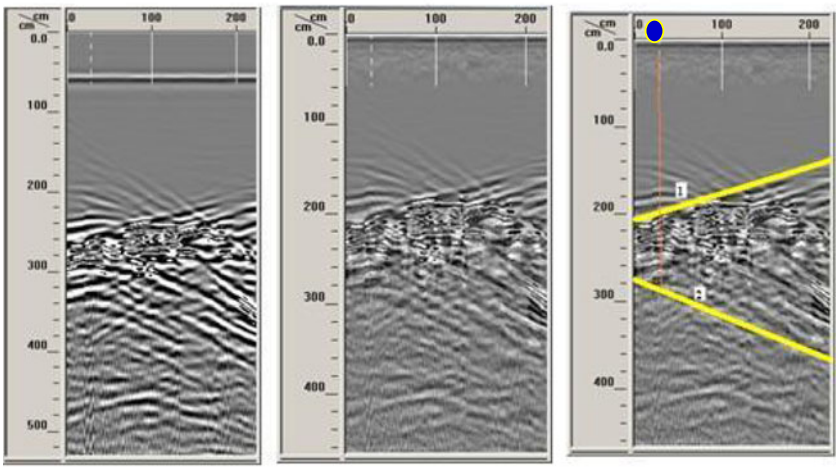

(B) Raw and processed GPR profile 2at Station 2

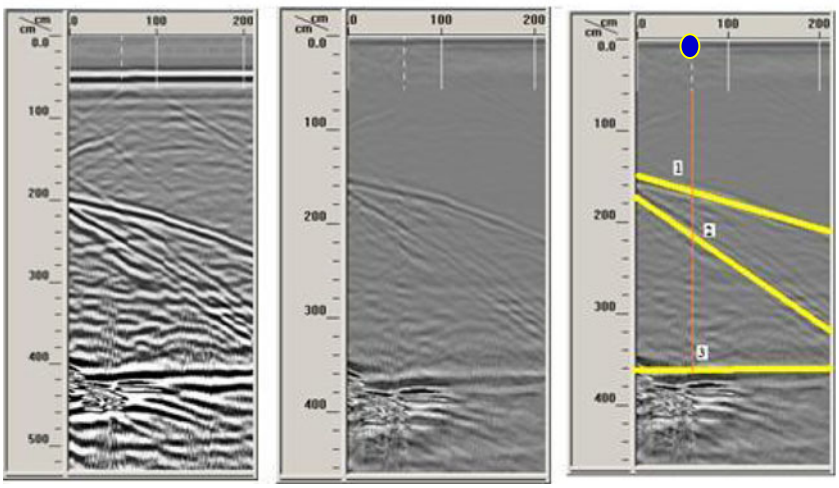

(C) Raw and processed GPR profile 1 at Station 3

Fig. 10 Raw (*left images*) and processed radiogram images (*middle images*) showing the detected hidden subvertical discontinuities in the study area with their apparent perpendicular depths (*right images*) measured from marked point 1 (*blue circle*)

α the apparent declination angle of the strike line of the detected hidden subvertical discontinuity.

Migration was applied as follows:

1. Apparent perpendicular horizontal depths (z) were estimated from radiogram images as shown in Figs. 10, 11, and 12 and listed in Tables 3, 4, and 5.
2. The apparent declination angles of the strike lines (α) of the detected hidden subvertical discontinuities were manually measured as shown in Fig. 12 and listed in Tables 3, 4, and 5.
3. The true declination angles of the strike lines (β) of the detected hidden subvertical discontinuities were estimated using Eq. 4 and as shown in Fig. 12 and listed in Tables 3, 4, and 5.

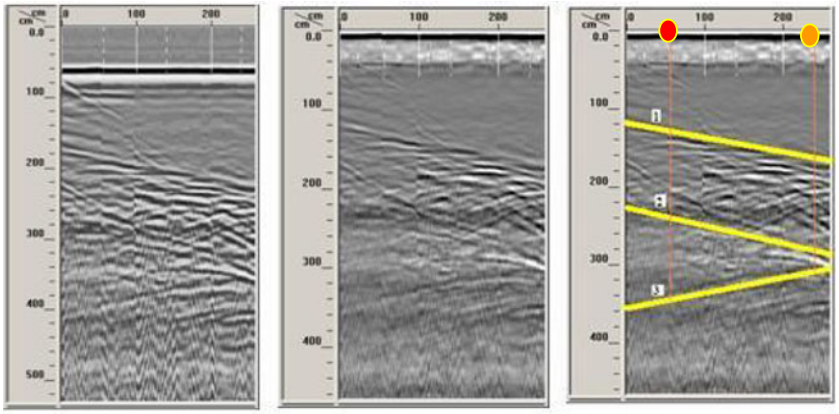

(A) Raw and processed GPR profile 4 at Station 1

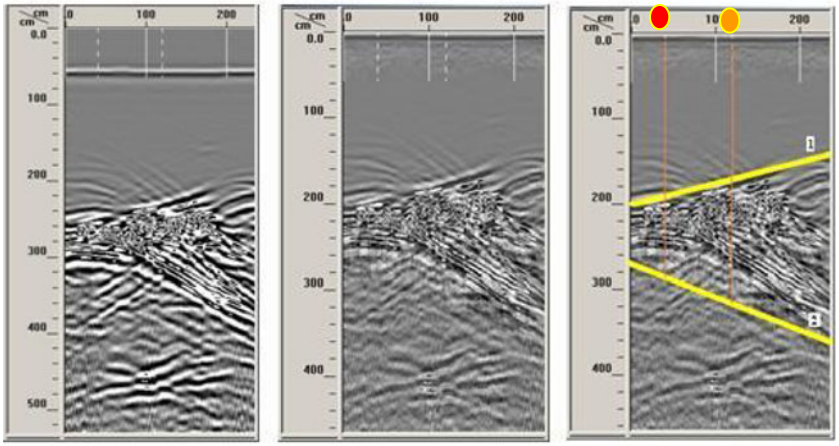

(B) Raw and processed GPR profile 1 at Station 2

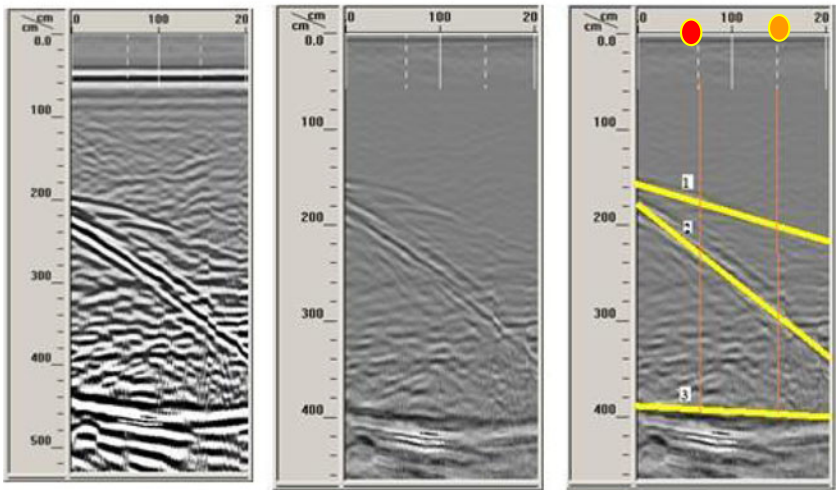

(C) Raw and processed GPR profile 6 at Station 3

Fig. 11 Raw (*left images*) and processed radiogram images (*middle images*) showing the detected hidden subvertical discontinuities in the study area with their apparent perpendicular depths (*right images*) measured from marked point 2 (*red circle*) and marked point 3 (*orange circle*)

4. True perpendicular horizontal depths (d) were estimated using the following equation:

$$d = z/\cos\beta \tag{5}$$

By estimating the true depths (d), migration can be done, and thus, true 3D images for the subvertical discontinuities in the study area can be generated (Figs. 13, 14, and 15).

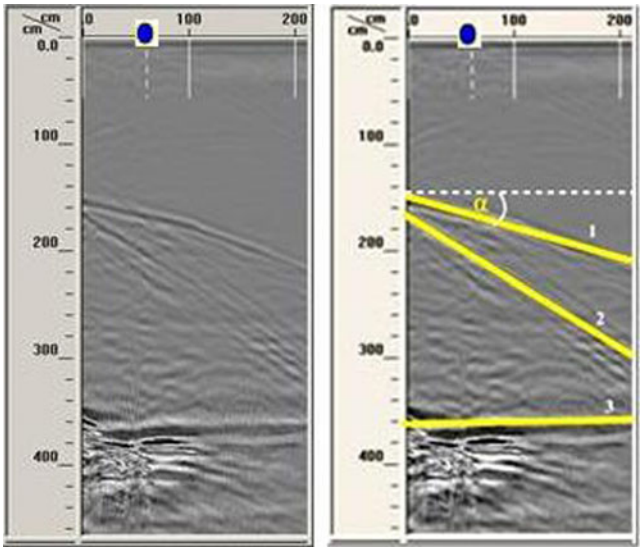

Fig. 12 The linear features in the radiograms represent the detected hidden subvertical discontinuities (*yellow lines*). The strike of joint no. 1 has an apparent declination angle (α) of 17° and also a true declination angle (β) of 17.80°

Results and field verifications

The hidden subvertical discontinuities were identified initially on the acquired 2D radiograms. Three hidden subvertical discontinuities were identified at each of both station 1and station 3, while two hidden subvertical discontinuities were identified at station 2 (Figs. 10 and 11). These hidden discontinuities were identified on all acquired and processed GPR survey profiles which are in a total of 18 GPR profiles. The apparent depths (z) were firstly estimated from these radiograms (Figs. 10 and 11) and then were recorded in Tables 3, 4, and 5.

Some of these detected joints intersect the rock-cut faces and could be visually identified in the field. Field verifications show that the linear trace of the detected hidden discontinuity 1 at station 3 is located at a depth of 154 cm (Fig. 3(d)), while the radiogram image in Fig. 10c shows that this linear trace is located at a depth of 150 cm. Moreover, field verifications indicate that there is no linear trace for the detected hidden discontinuity 2 at a depth of 173 cm (Fig. 3(d)) as shown in the radiogram image (Fig. 10c). Furthermore, the same thing was noted for station 2 where field verifications indicate that the linear traces of discontinuities 1 and 2 are located at depths of 217 and 294 cm, respectively (Fig. 3(c)), while the radiogram

Table 3 The apparent and true horizontal perpendicular depths from the rock-cut face to the detected hidden subvertical discontinuities at station 1

Discontinuity no.	Apparent horizontal perpendicular depths (z) from the 3 points on the rock-cut face of station 1, in cm			Apparent (α) and true (β) declination angles of the strike		True horizontal perpendicular depths (d) from the 3 points on the rock-cut face of station 1, in cm		
	Point 1	Point 2	Point 3	α	β	Point 1	Point 2	Point 3
1	148	133	170	11°	11.2°	151	136	173
2	261	234	282	16°	16.7°	272	244	294
3	325	344	314	10°	10.2°	330	350	319

Table 4 The apparent and true perpendicular depths from the rock-cut face to the detected hidden subvertical discontinuities at station 2

Discontinuity no.	Apparent horizontal perpendicular depths (z) from the 3 points on the rock-cut face of station 2, in cm			Apparent (α) and true (β) declination angles of the strike		True horizontal perpendicular depths (d) from the 3 points on the rock-cut face of station 2, in cm		
	Point 1	Point 2	Point 3	α	β	Point 1	Point 2	Point 3
1	188	198	177	16°	16.7°	196	207	185
2	287	285	318	22°	23.8°	314	311	348

Table 5 The apparent and true horizontal perpendicular depths from the rock-cut face to the detected hidden subvertical discontinuities at station 3

Discontinuity no.	Apparent horizontal perpendicular depths (z) from the 3 points on the rock-cut face of station 3, in cm			Apparent (α) and true (β) declination angles of the strike		True horizontal perpendicular depths (d) from the 3 points on the rock-cut face of station 3, in cm		
	Point 1	Point 2	Point 3	α	β	Point 1	Point 2	Point 3
1	165	172	206	17°	17.8°	173	181	216
2	208	223	290	35°	44.4°	291	312	406
3	364	396	404	03°	03°	364	396	404

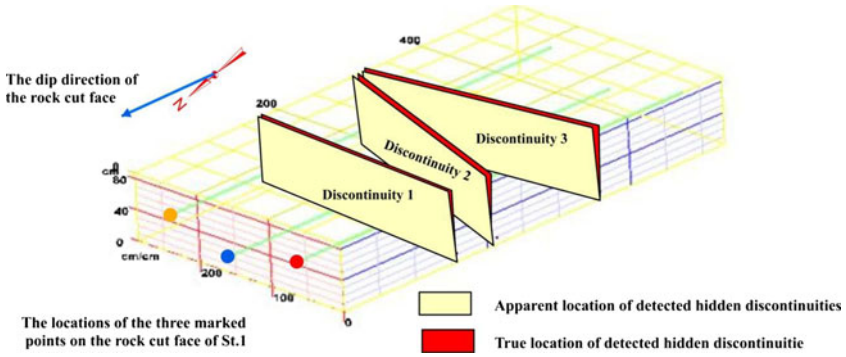

Fig. 13 The created 3D image of station 1 using RADAN software and ArcGIS showing the location of the detected hidden subvertical discontinuities

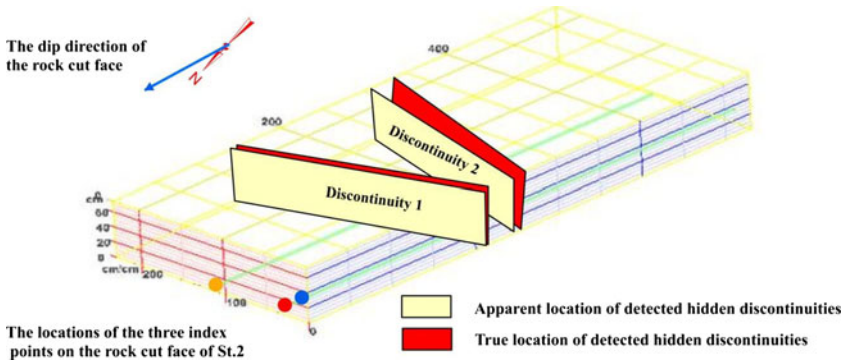

Fig. 14 The created 3D image of station 2 using RADAN software and ArcGIS showing the location of the detected hidden subvertical discontinuities

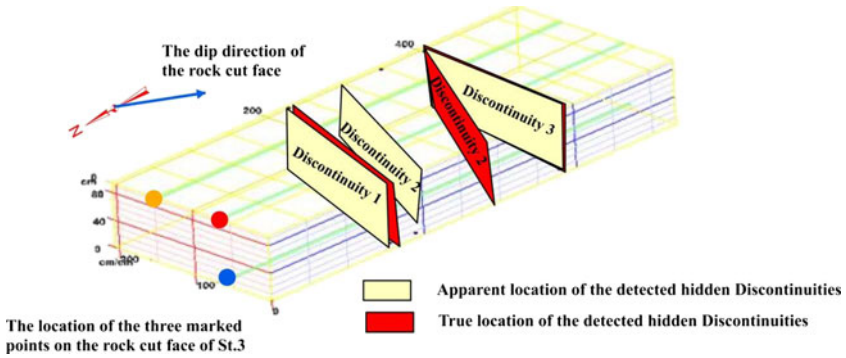

Fig. 15 The created 3D image of station 3 using RADAN software and ArcGIS showing the location of the detected hidden subvertical discontinuities

image shows that the two detected hidden discontinuities are located at depths of 210 and 287 cm, respectively (Fig. 10b).

As a result, migration of the GPR data was a necessary step to relocate the detected discontinuities to estimate the true depths and to create 3D true images (Figs. 13, 14, and 15) as explained in the previous section. Based on the analysis of Figs. 13, 14, and 15, the following observations can be made and then conclusions can be drawn:

- The true perpendicular horizontal depths (d) of the hidden discontinuity 1 and discontinuity 2 at station 2 as shown in Fig. 14 match the field verification measurements.
- The true perpendicular horizontal depths of the hidden discontinuity 1 at station 3 as shown in Fig. 15 match the field verification measurements.
- The detected discontinuity 2 at station 3 (Figs. 3(d) and 10c) does not intersect the exposed rock.
- It was not possible to make field verification measurements for the detected discontinuities at station 1. However, it can be considered that the results of station 1 are reasonable and acceptable according to the results obtained from both station 2 and station 3.

Conclusions

The results show that GPR can be used to detect and map discontinuities in rock masses. GPR antenna with appropriate frequency given the depth of the target and breadth of the discontinuity should be employed. The utilized 400-MHz antenna, in this research, showed the ability to optimize between depth of penetration and required resolution to clearly identify and map hidden discontinuities in highway sandstone rock cuts. Discontinuities with apertures even less than a 1-cm width can be identified at about 4 m of depths in sandstone rock cuts but by utilizing a 400-MHz monostatic GPR antenna. Manual migration can be successfully used to reconstruct the geometry of the hidden subvertical discontinuities in rock cuts, but GPR signal velocity has to be estimated accurately first.

Information about the pattern, placement, and density of fractures within a rock mass can be used for rock slope stability analysis and rock engineering purposes. Such information may increase the degree of confidence and, thus, the accuracy of predicting rock failures and their mode of failures, too.

Acknowledgments We would like to thank both the Rock Mechanics and Explosive Research Center and the Geological Engineering Program at the Missouri University of Science (USA) for their technical assistance.

References

Annan AP (2009) Electromagnetic principles of ground penetrating radar. In: Jol HM (ed) Ground penetrating radar: theory and applications, 2009. Elsevier, Solvenia, pp 4–40

Aqeel AM (2012) Measuring the orientations of hidden subvertical joints in highways rock cuts using ground penetrating radar in combination with LIDAR. Dissertation, Missouri University of Science and Technology

Bieniawski ZT (1989) Engineering rock mass classification: a complete manual for engineers and geologists in mining, civil, and petroleum engineering. Wiley, Canada

Beres M Jr, Haeni FP (1991) Application of ground-penetrating-radar methods in hydrogeologic studies. Ground Water 29(3):375–386

Booth AD, Endres AL, Murray T (2009) Spectral bandwidth enhancement of GPR profiling data using multiple-frequency compositing. J Appl Geophys 67:88–97

Cassidy NJ (2009a) Electrical and magnetic properties of rocks, soils and fluids. In: Jol HM (ed) Ground penetrating radar: theory and applications, 2009. Elsevier, Solvenia, pp 41–66

Cassidy NJ (2009b) Ground penetrating radar data processing, modelling, and analysis. In: Jol H (ed) Ground penetrating radar: theory and applications, 2009. Elsevier, Solvenia, pp 141–171

Chernyshev SN, Dearman WR (1991) Rock fractures. Butterworth-Heinemann Ltd, London

Conyers LB (2004) Ground-penetrating radar for archaeology. Altamira, Walnut Creek

Daniels DJ (2004) Ground penetrating radar, 2nd edn. Institution of Electrical Engineers, London

Donovan J, Kemeny J, Handy J. The application of three-dimensional imaging to rock discontinuity characterization, Alaska Rocks, Proceedings of the 40th US Rock Mechanics Symposium, Anchorage Alaska, June 25–29 2005; 7 pp

Duan Y, Xiaoling L, Maerz N, Otto J (2011) Automatic 3D facet orientation from LIDAR imaging. Proceedings of 2011 NSF engineering research and innovation conference. Atlanta, Georgia, USA

Haneberg W (2008) Using close range terrestrial digital photogrammetry for 3-D rock slope modeling and discontinuity mapping in the United States. Bull Eng Geol Environ 67(4):457–469

Jenyon M K, Fitch A (1985) Seismic reflection interpretation Gebrüder Borntraeger, Berlin

Kleyn AH (1983) Seismic reflection interpretation. Applied Science, England

Kiliche CA (1999) Rock slope stability. Society for Mining, Metallurgy, and Exploration, Englewood

Kovin O, Anderson N (2005) Use of ground penetrating radar for fracture imagining. Appl. Geophysics Conference, p: 566–573

Kovin O, Anderson N (2006) Use of ground penetrating radar for fracture imagining. Geophys. 78, NO. 3 (10), p: 91–103

Kovin O (2010) Ground Penetrating Radar Investigation in Upper Kama Potash Mines. Dissertation, Missouri University of Science and Technology

Lines LR, Newrick RT (2004) Geophysical monograph series, No.13: Fundamentals of geophysical interpretation. Society of Exploration Geophysicist, Tulsa

Maerz NH, Kim W (2000) Potential use of ground penetrating radar in highway rock cut stability. Geophysics conference, St. Louis, MO, 9 pp

Otoo JN, Maerz NH, Duan Y, Xiaoling L (2011a) 3-D discontinuity orientations using combined optical imaging and LiDAR techniques. The 45th US Rock Mechanics/Geomechanics Symposium, June 26–29, San Francisco, CA, USA

Otoo JN, Maerz NH, Duan Y, Xiaoling L (2011b) LiDAR and optical imagining for 3-D fracture orientations. Proceedings of 2011 NSF engineering research and innovation conference. Atlanta, Georgia, USA

Otto JC, Sass O (2006) Comparing geophysical methods for talus slope investigations in the Turtmann Valley (Swiss Alps). Geomorphology 76:257–277

Porsani J, Sauck W, Junior A (2006) GPR for mapping fractures and as a guide for the extraction of ornamental granite from a quarry: a case study from southern Brazil. J Appl Geophys 58:177–187

Post R (2001) Characterizing of joints and fractures in a rock mass using digital image processing. M.S. Thesis, University of Arizona

Priest SD (1993) Discontinuity analysis for rock engineering. Chapman and Hall, London

Reynolds JM (1997) An introduction to applied and environmental geophysics. Wiley, London

Sass O (2007) Bedrock detection and talus thickness assessment in the European Alps using geophysical methods. J Appl Geophys 62:254–269

Scheidegger AE (1978) The enigma of jointing, Rivista Italiana Di Geofisica, 1–4

Slob S, Hack R (2004) 3D terrestrial laser scanning as a new field measurement and monitoring technique. Eng Geol Infrastructure Planning Europe 103:179–189

Slob S, Hack H, Van Knapen B, Kemeny J (2004) Automated identification and characterization of discontinuity sets in outcropping rock masses using 3D terrestrial laser scan survey techniques. In: Essen WS, Verlag GIA K (eds) Proceedings of the ISRM regional symposium EUROCK, 2004 and 53rd geomechanics colloquy: rock engineering and practice, October 7–9, Salzburg, Austria, 439–443

Slob S, Hack HRGK, Van Knapen B, Turner K, Kemeny J (2005) A method for automated discontinuity analysis of rock slopes with 3D laser scanning. In: Proceedings of the Transportation Research Board (TRB) 84th annual meeting, January 9–13, 2005 Washington D.C. Transp Res Rec 1913:187–194

Soel S, Kim J, Song Y, Chung S (2001) Finding the strike direction of fractures using GPR. Geophys Prospect 49:300–308

Sturzeinegger M, Stead D (2009) Close-range terrestrial digital photogrammetry and terrestrial laser scanning for discontinuity characterization on rock cuts. Eng Geol 106:163–182

Takahashi T (2004) ISRM suggested methods for land geophysics in rock engineering. Int J Rock Mech Min Sci 41:885–914